

## Article

# Degradation of Mechanical Behavior of Sandstone under Freeze-Thaw Conditions with Different Low Temperatures

Jingwei Gao, Chao Xu, Yan Xi and Lifeng Fan \*

College of Architecture and Civil Engineering, Beijing University of Technology, Beijing 100124, China; gaojingweibjut@163.com (J.G.); xuchaobjut@126.com (C.X.); xiyan@bjut.edu.cn (Y.X.)

\* Correspondence: fanlifeng@bjut.edu.cn

**Abstract:** This study investigated the effects of freezing temperature under freeze-thaw cycling conditions on the mechanical behavior of sandstone. First, the sandstone specimens were subjected to 10-time freeze-thaw cycling treatments at different freezing temperatures (−20, −40, −50, and −60 °C). Subsequently, a series of density, ultrasonic wave, and static and dynamic mechanical behavior tests were carried out. Finally, the effects of freezing temperature on the density, P-wave velocity, stress–strain curves, static and dynamic uniaxial compressive strength, static elastic modulus, and dynamic energy absorption of sandstone were discussed. The results show that the density slightly decreases as temperature decreases, approximately by 1.0% at −60 °C compared with that at 20 °C. The P-wave velocity, static and dynamic uniaxial compressive strength, static elastic modulus, and dynamic energy absorption obviously decrease. As freezing temperature decreases from 20 to −60 °C, the static uniaxial compressive strength, static elastic modulus, dynamic strength, and dynamic energy absorption of sandstone decrease by 16.8%, 21.2%, 30.8%, and 30.7%, respectively. The dynamic mechanical behavior is more sensitive to the freezing temperature during freeze-thawing cycling compared with the static mechanical behavior. In addition, a higher strain rate can induce a higher dynamic strength and energy absorption.

**Keywords:** freezing temperature; freeze-thaw cycles; mechanical behavior; sandstone



**Citation:** Gao, J.; Xu, C.; Xi, Y.; Fan, L. Degradation of Mechanical Behavior of Sandstone under Freeze-Thaw Conditions with Different Low Temperatures. *Appl. Sci.* **2021**, *11*, 10653. <https://doi.org/10.3390/app112210653>

Academic Editors: Hao Cheng, Yundong Shou, Junwei Chen and Xiaoping Zhou

Received: 7 October 2021  
Accepted: 10 November 2021  
Published: 12 November 2021

**Publisher's Note:** MDPI stays neutral with regard to jurisdictional claims in published maps and institutional affiliations.



**Copyright:** © 2021 by the authors. Licensee MDPI, Basel, Switzerland. This article is an open access article distributed under the terms and conditions of the Creative Commons Attribution (CC BY) license (<https://creativecommons.org/licenses/by/4.0/>).

## 1. Introduction

In cold regions, the rock generally suffers from freeze-thaw cycling action induced by the environment temperature change. Freeze-thaw cycling action induces the accumulation of damage in rock, which further causes the degradation of strength of rock and the decrease in the stability and safety of engineering [1–3]. The rock in different areas experiences different levels of freezing temperature in the freeze-thaw cycling process [4,5]. Therefore, investigation of the relationship between mechanical behaviors of rock and freezing temperature under repeated freezing and thawing conditions is necessary.

The relationship between the mechanical behavior of rock and freezing temperature under freezing conditions has been extensively studied. A series of physical and mechanical behavior tests have been conducted on the rock specimens under the freezing conditions, including the ultrasonic wave test [6], the uniaxial compression test [7], the indirect tensile test [8], the triaxial compression test [9], the fracture toughness test [10], the dynamic tensile test [11], and the dynamic compression test [12]. The result shows that the larger differences between the mechanical behavior of frozen rock specimens and original specimens exist. Under the freezing conditions, the mechanical strength, static elastic modulus, and P-wave velocity of rock specimens generally increase as freezing temperature decreases. In addition, some researchers found as freezing temperature decreases, the mechanical strength of rock specimen first shows an increasing trend and then shows a decreasing trend below a critical temperature [13,14]. Some researchers found that the mechanical strength of rock first decreases and then increases as the temperature decreases [15,16]. The effects of the freezing temperature under freezing conditions on the physical and mechanical behaviors

of rock are complicated. The complicated mechanical responses may be related to the co-existence of the water and ice in the pores. The water has weakening effects [17]. The water content decreases as temperature decreases, and the ice content increases [18]. The increase in the content of the ice filling in the pores can induce an increase in the strength of rock to a certain extent [19]. In this case, the ice has strengthening effects. Water–ice phase transition approximately induces a 9% volume increase. When the frost heaving force induced by the volume expansion of the ice in pores exceeds the strength of the material, the micro-defects are generated and accumulated in rock [2]. In this case, the ice has weakening effects. Therefore, the complicated mechanical responses of the rock may depend on whether the ice-strengthening effects prevailed over the water-weakening effects and ice-weakening effects or not. In practice, the rock is subjected to not only the freezing action but also the freeze-thaw cycling action.

The relationship between the mechanical behavior of rock and cycling number under repeated freezing and thawing conditions has been also extensively studied. A series of physical and mechanical behavior tests have been conducted on the rock specimens after freeze-thaw cycling treatments [20–22]. Research shows P-wave velocity and mechanical strength show a decreasing trend with the increase in the cycling number [23–25]. In dynamic mechanics behavior tests, the dynamic energy absorption decreases as the freeze-thawing cycles increase [26,27]. Based on microscopic observation, the weakening of rock is related to the increase in micro defects and the propagation of original micro defects during freeze-thaw cycling [28–30]. Under the repeated freezing-thawing conditions, the volume expansion, due to the water–ice phase change, may induce a frost heave force in the freezing phase. When the frost heave force exceeds the strength of the material, the micro-defects are generated. In addition, the inconsistent contraction and expansion between mineral grains during freezing and thawing may also induce the generation of stress, which further may induce sub-critical crack growth or fatigue cracking, and cause the material properties to deteriorate [31–34].

Previous studies pay more attention to the effects of freezing temperature under the freezing condition and the effects of cycling number under the freeze-thaw cycling condition. However, the studies about the effect of freezing temperature under the freeze-thaw cycling conditions on mechanical behaviors of rock are relatively limited and concentrated on the static mechanical behavior [4,5,35]. The P-wave velocity and mechanical strength decrease as the freezing temperature during freeze-thaw cycling decreases [36]. In cold region engineering, the rock in different areas experiences different levels of freezing temperature in the freeze-thaw cycling process, and these rocks generally suffer from dynamic loading induced by drilling-induced vibration, underground explosion, and earthquake [37,38]. Therefore, further studying the variation of dynamic mechanical behaviors of rock with freezing temperature under repeated freezing and thawing conditions is necessary. Under the repeated freezing and thawing conditions, the influences of the freezing temperature on the dynamic mechanical behaviors, including P-wave velocity, dynamic compression strength, and dynamic energy absorption, need to be further studied.

This study aims to investigate the degradation of the mechanical behavior of sandstone with freeze temperature under freeze-thaw conditions in terms of stress–strain curves, static uniaxial compressive strength, static elastic modulus, dynamic strength, and dynamic energy absorption. This study is expected to provide a safe design and stability evaluation guidance in rock mass engineering in cold regions.

## 2. Materials and Methods

### 2.1. Specimen Preparation

Sandstone is a common rock in cold region engineering. The sandstone in the present study originated from Sichuan Province, China. The X-ray diffraction (XRD) test was conducted on the sandstone to obtain its mineralogical compositions, using the D8-ADVANCE X-ray diffractometer. Figure 1a shows the mineralogical compositions of sandstone. It is seen from Figure 1a that quartz and clay are the main mineral compositions of sandstone,

and that the proportion of quartz mineral reaches 93.2% and the proportion of clay mineral is 6.8%.

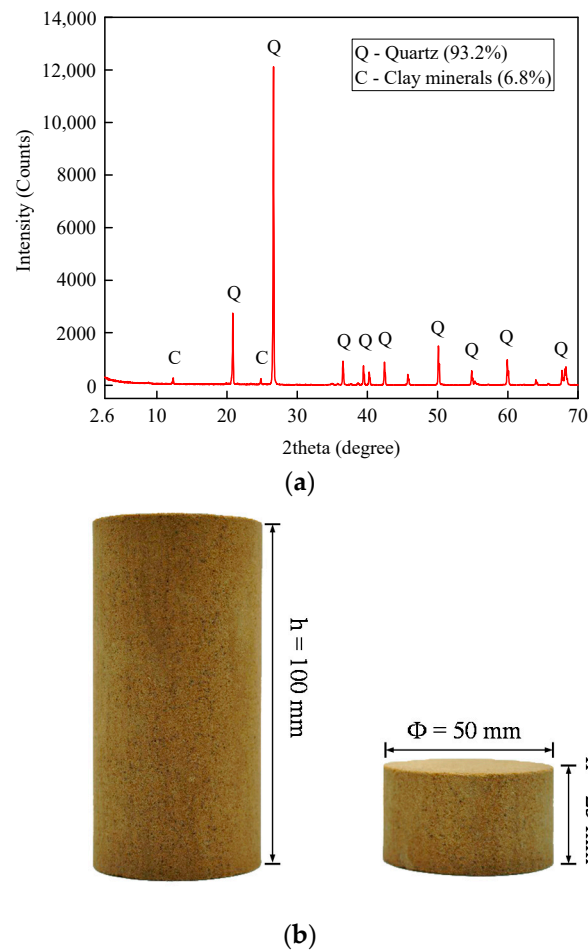


**Figure 1.** Specimen preparation. (a) Mineralogical compositions of sandstone. (b) Sandstone specimens.

The preparation process of specimens followed the procedures provided by the International Society of Rock Mechanics (ISRM), which is a suggested method for mechanical behavior tests [39,40]. Figure 1b shows sandstone specimens used in the present study. The cylindrical specimen was prepared for density, P-wave velocity, and static uniaxial compression test, and its diameter and length were 50.0 mm and 100.0 mm, respectively. The disc specimen was prepared for split Hopkinson pressure bar (SHPB) tests, and its diameter and thickness were 50.0 mm and 25.0 mm, respectively. Two end faces of the specimen were carefully polished for ensuring their parallelism, and the end face roughness was less than 0.02 mm. Sandstone specimens used in the experiment should be cored along the same direction in a huge rock block to avoid anisotropy influences [41,42].

Before freeze-thaw cycling treatments, dry treatments and water saturation treatments were conducted on all sandstone specimens, respectively [25,27]. First, dry treatments were performed on all specimens at 105 °C for 48 h. Next, under room temperature conditions, these specimens after drying treatments were completely submerged in water for 48 h. Finally, these specimens were saturated at  $-0.095$  MPa for 8 h using the vacuum water saturation instrument.

## 2.2. Freeze-Thaw Cycling Treatments

Repeated freezing and thawing were performed on the saturated specimens. The GDW-100 low-temperature test chamber for freezing treatments was used in the freeze-

thaw cycling processes, which can supply the temperature range from  $-70$  to  $50$  °C. In the freezing processes of specimens, the freezing temperature level in a low-temperature test chamber can be controlled programmatically.

The ice content in the ice–water mixture increases as temperature decreases under the negative temperature environment, and the ice content can reach 90% at  $-50$  °C [13]. Therefore, in the present study, the minimum freezing temperature was set as  $-60$  °C. Four different freezing temperature levels (i.e.,  $-20$ ,  $-40$ ,  $-50$ , and  $-60$  °C) were considered in the present study. In addition, the room temperature level ( $20$  °C), as a control group, was also considered. Both of the cylindrical specimens and the disc specimens were divided into five groups according to the freezing temperature level and the room temperature level. For the specimens subjected to freeze-thaw cycling treatments, each group of specimens was first kept at the corresponding freezing temperature for 8 h using the low-temperature test chamber and then were taken out from the low-temperature test chamber to be submerged in water for 16 h at room temperature. This is one complete freeze-thaw cycle, which lasted 24 h. Ten freeze-thaw cycles were conducted on each group of specimens. For the specimens in the control group without experiencing freeze-thaw cycling treatments, they were first dried naturally under the condition of room temperature for 8 h and then were submerged in water under the condition of room temperature for 16 h, which was one dry–wet cycle. The specimens in the control group were treated by 10 dry–wet cycles.

After freeze-thaw cycling treatments, firstly, dry treatments at  $105$  °C for 48 h were performed on all specimens to avoid the influence of the different moisture content on experimental results. Subsequently, the quality and volume measurements were conducted on the cylindrical specimens to calculate the density of the specimen, and the effect of freezing temperature on density was studied. After the density test, ultrasonic wave tests were carried out. The damage degree of specimens can be reflected by the change in ultrasonic wave velocity [43]. After density and P-wave velocity tests, the static uniaxial compression and SHPB tests were carried out, respectively.

### 2.3. Static Uniaxial Compression Tests

Figure 2a shows the SHT4605 uniaxial compressive testing device with a maximum loading of 600 kN in Beijing University of Technology, China. Based on this mechanical testing machine, the static uniaxial compressive behaviors of sandstone after freeze-thaw cycling treatments with different freezing temperatures were tested. The displacement loading mode was used in the present study. The loading rate was 0.50 mm/min.

### 2.4. SHPB Tests

The SHPB tests were conducted on the disc specimens after freeze-thaw cycling treatments with different freezing temperatures. Figure 2b shows the sketch map of the SHPB system, which includes a gas gun, a striker bar, an incident bar, a transmitted bar, an absorbed bar, a damper, strain gauges, a strainmeter, and a data-processing unit. Both of the diameters of the incident bar and transmitted bar were 100 mm. The lengths of the incident bar and transmitted bar were 4000 mm and 3000 mm, respectively. The elastic modulus of the bar is 190 GPa. During the SHPB tests, the strain gauge on the incident bar was used to record incident waves and reflected waves. The transmitted wave was recorded by the strain gauge on the transmitted bar.

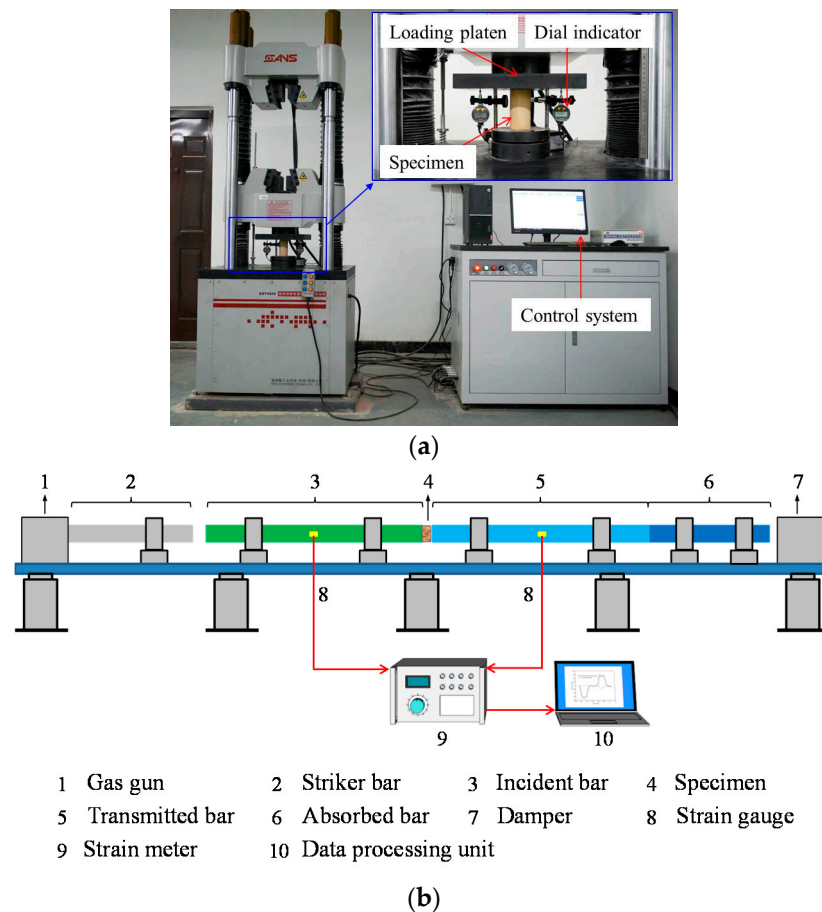


**Figure 2.** Experimental devices. (a) Uniaxial compressive testing machine. (b) Schematic diagram of SHPB apparatus.

After the SHPB tests, the strain rate  $\dot{\epsilon}(t)$ , strain  $\epsilon(t)$ , and stress  $\sigma(t)$  of specimens can be derived, according to the methods suggested by ISRM [40,44].

$$\begin{cases} \dot{\epsilon}(t) = -\frac{2C_0}{L}\epsilon_r(t) \\ \epsilon(t) = -\frac{2C_0}{L}\int_0^t \epsilon_r(t)dt \\ \sigma(t) = \frac{A}{A_S}E\epsilon_t(t) \end{cases} \quad (1)$$

where  $L$  and  $A_S$  are the length and cross-sectional area of the specimen, respectively.  $A$ ,  $C_0$ , and  $E$  are the cross-sectional area, elastic wave velocity, and Young’s modulus of the bar, respectively.  $\epsilon_r(t)$  and  $\epsilon_t(t)$  are the strain of reflected wave and transmitted wave, respectively.

The velocity of the striker bar can be changed by charging different levels of pressures in the gas gun, which further vary the strain rate on the specimen [45]. The impact pressure in each group of experiments was set to 0.055 MPa, and then the variation of dynamic mechanical behavior of sandstone specimens with freezing temperature was studied. In addition, different impact pressures were applied on the specimens subjected to 10-times freeze-thaw cycling treatments with a freezing temperature of  $-40\text{ }^\circ\text{C}$ . The variation of mechanical behavior of sandstone specimens after freeze-thaw cycling treatments with strain rate was also studied. The impact pressures applied on the specimens were 0.050, 0.055, and 0.060 MPa, respectively.

### 3. Results

#### 3.1. Effects of Freezing Temperature on Density and P-Wave Velocity

The relationship between the density and freezing temperature under the same number of freezing–thawing cycles is shown in Figure 3. The density slightly decreases with decreasing temperature from 20 to  $-60$  °C, and the decreasing extent of density approximately reaches 1.0% at  $-60$  °C.

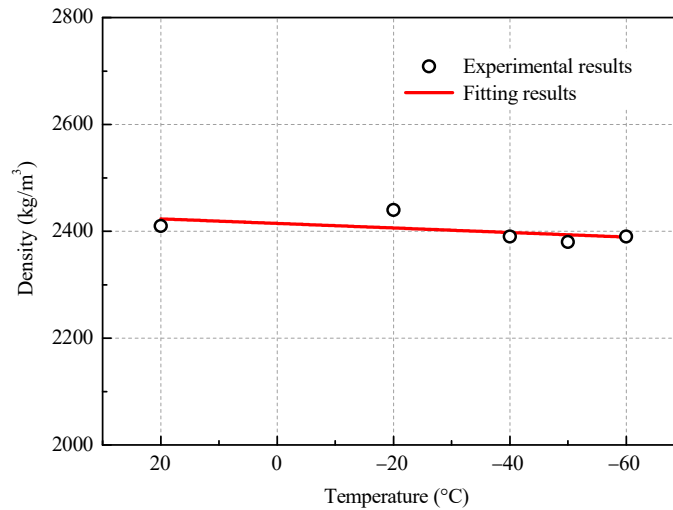


Figure 3. Variation of density with freezing temperature.

Figure 4 shows the effects of freezing temperature on P-wave velocity. The P-wave velocity first slightly decreases with the decrease in freezing temperature, and then the rate of decrease in P-wave velocity rapidly increases below  $-20$  °C. Compared with the P-wave velocity at 20 °C, the P-wave velocity at the freezing temperature of  $-40$ ,  $-50$ , and  $-60$  °C decreases by 7.7%, 12.8%, and 14.5%, respectively.

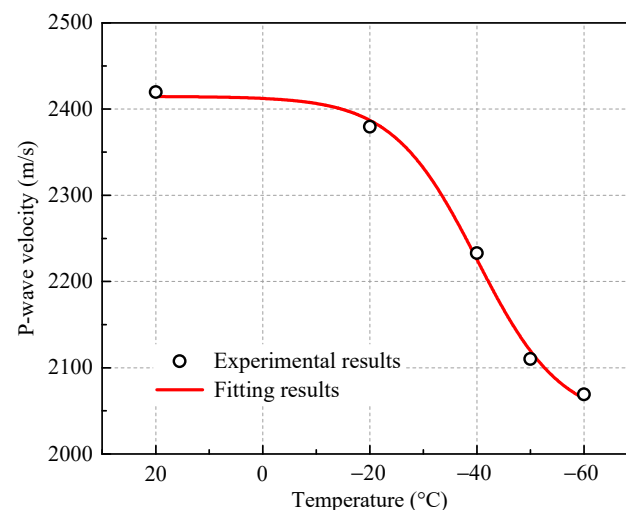
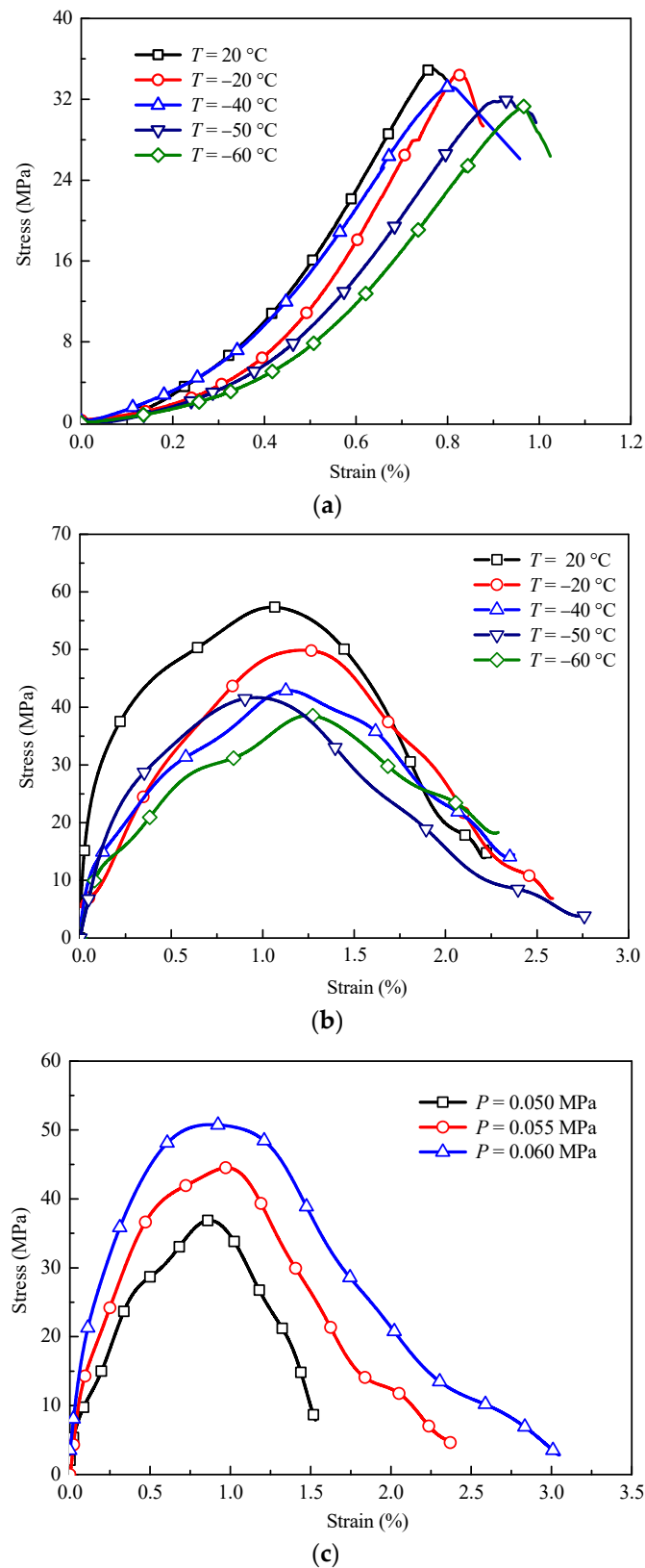


Figure 4. Variation of P-wave velocity with freezing temperature.

#### 3.2. Effects of Freezing Temperature and Impact Pressure on the Stress–Strain Curve

The stress–strain response of rock gives a fundamental understanding of the mechanical behavior of rock. Figure 5 shows the static and dynamic stress–strain curves of the specimen after freeze–thaw cycling treatments.



**Figure 5.** Stress–strain curves. (a) Static stress–strain curves at different freezing temperature. (b) Dynamic stress–strain curves at different freezing temperature. (c) Dynamic stress–strain curves at different impact pressures.

Figure 5a shows the effects of freezing temperatures during the freeze-thaw cycling process on the static stress–strain curves. The static stress–strain curves mainly experience

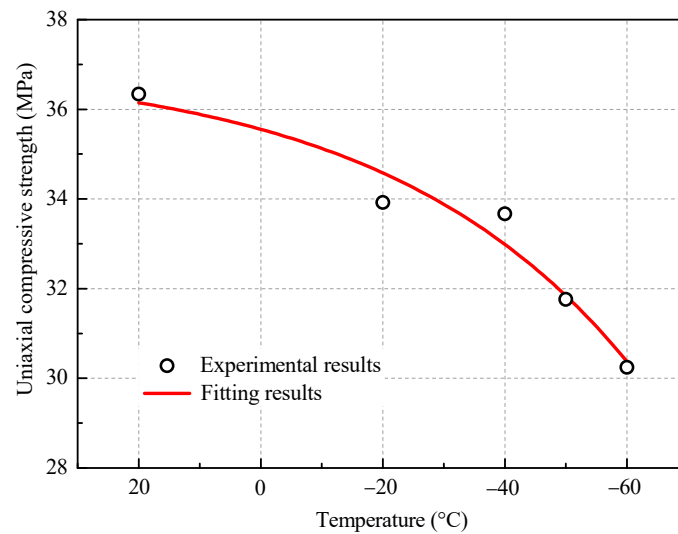
four stages: compaction, elastic deformation, yielding deformation, and failure at different freezing temperatures. In the compaction stage, the stress increases non-linearly as the strain increases, and the stress–strain shape is approximately concave. The compaction stage during loading may be induced by the closure of pre-existing micro-pores and micro-defects [46]. In the elastic stage, the stress increases almost linearly as the strain increases. In the yield stage, the stress increases non-linearly as the strain increases and reaches a peak, and the stress–strain curve shape is approximately convex. The peak stress is used as the uniaxial compressive strength of the sandstone. The peak stress in these static stress–strain curves decreases as the freezing temperature decreases. In the failure stage, the specimen is quickly destroyed after the peak stress is reached.

Figure 5b shows the effects of freezing temperatures during freeze-thaw cycling on the dynamic stress–strain curves. The dynamic stress–strain curves mainly experience three stages: elastic deformation, yielding deformation, and failure at different freezing temperatures. The compaction stage in the dynamic stress–strain curve is not obvious compared with the static stress–strain curve, which may be because the pores in the sandstone are too late to close under the dynamic load conditions, and the resistance to deformation is improved [47]. In the elastic stage, the stress increases almost linearly as the strain increases. In the yield yielding stage, the stress increases non-linearly as the strain increases and reaches a peak. The peak stress in the dynamic stress–strain curve is used as the dynamic compressive strength of the sandstone. The peak stress decreases as freezing temperature decreases. In the failure stage, the stress decreases as the strain further increases, and the rock breaks in this stage.

Figure 5c shows the effects of impact pressures on dynamic stress–strain curves of specimens experiencing 10-times freezing and thawing cycles with freezing temperature of  $-40\text{ }^{\circ}\text{C}$ . The stress–strain curves mainly experience three stages: elastic deformation, yielding deformation, and failure at different impact pressures. The compaction stages in the dynamic stress–strain curves are not obvious at the three different impact pressures. In the elastic stage, the stress increases almost linearly as the strain increases, and the slope of the line is used as the dynamic elastic modulus. The dynamic elastic modulus increases as the impact pressure increases. In the yielding stage, the stress increases non-linearly as the strain increases and reaches the peak, and the peak stress increases as the impact pressure increases. In the failure stage, the stress decreases as the strain further increases, and the rock breaks in this stage. The total strain increases as the impact pressure increases.

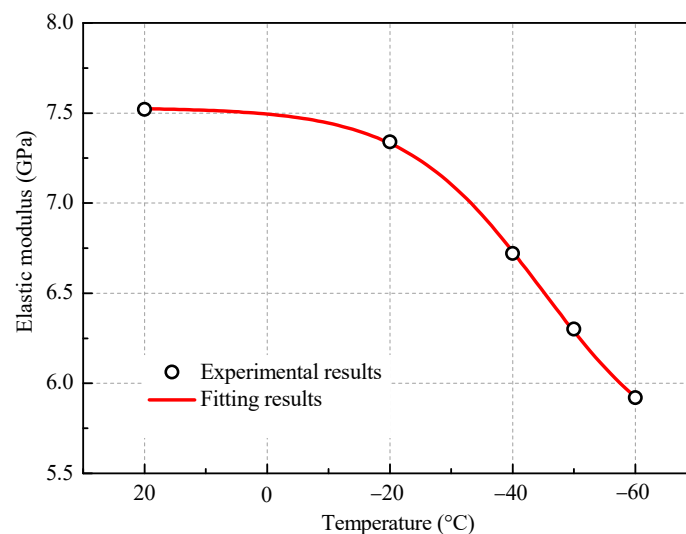
### *3.3. Effects of Freezing Temperature on Static Uniaxial Compressive Strength and Static Elastic Modulus*

The relationship between the static uniaxial compressive strength and freezing temperature during the freeze-thaw cycling process is shown in Figure 6. It is seen from Figure 6 that, as the temperature decreases, the uniaxial compressive strength decreases. Compared with the uniaxial compressive strength at  $20\text{ }^{\circ}\text{C}$ , the uniaxial compressive strength at the freezing temperature of  $-20$ ,  $-40$ ,  $-50$ , and  $-60\text{ }^{\circ}\text{C}$  decreases by 6.7%, 7.4%, 12.6%, and 16.8%, respectively.



**Figure 6.** Variation of static uniaxial compressive strength with freezing temperature.

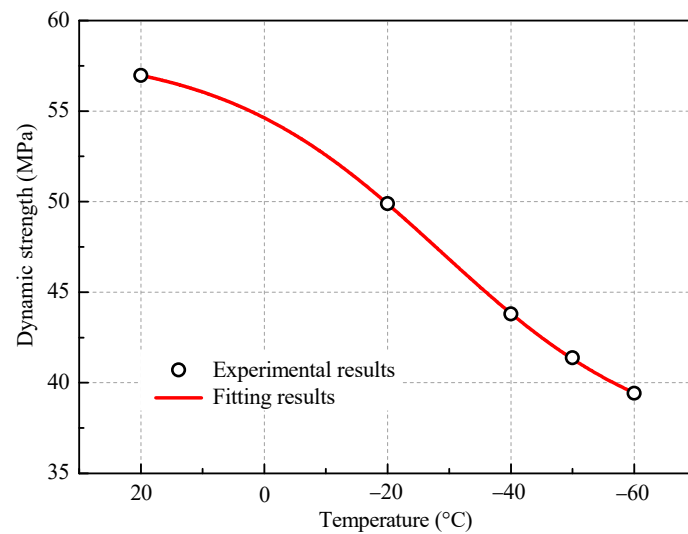
The relationship between the static elastic modulus and freezing temperature during the freeze-thaw cycling process is shown in Figure 7. The static elastic modulus first slightly decreases as the freezing temperature decreases, and the rate of decrease in the elastic modulus rapidly increases after  $-20$  °C. Compared with the static elastic modulus at  $20$  °C, the static elastic modulus at the freezing temperature of  $-40$ ,  $-50$ , and  $-60$  °C decreases by 10.6%, 16.2%, and 21.3%, respectively.



**Figure 7.** Variation of static elastic modulus with freezing temperature.

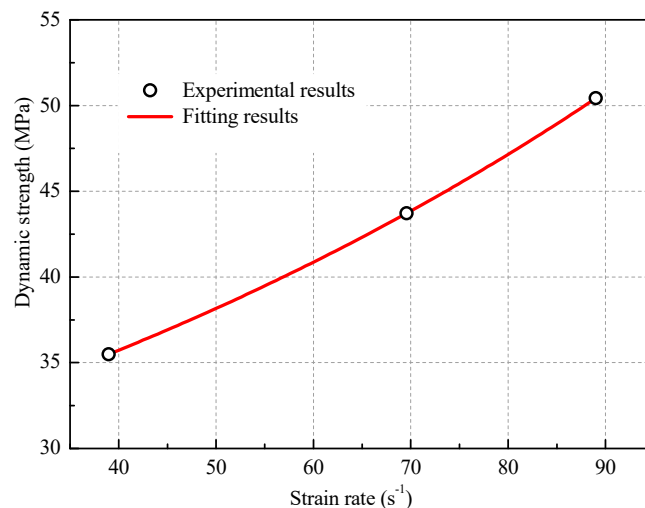
### 3.4. Effects of Freezing Temperature and Strain Rate on Dynamic Strength

Figure 8 shows the relationship between the dynamic strength of sandstone specimens and freezing temperature under the same freeze-thaw cycling number. As the freezing temperature decreases, the dynamic strength decreases. Compared with the dynamic strength at  $20$  °C, the dynamic strength at the freezing temperature of  $-20$ ,  $-40$ ,  $-50$ , and  $-60$  °C decreases by 12.4%, 23.1%, 27.4%, and 30.8%, respectively. The dynamic mechanical behavior is more sensitive to the freezing temperature during freeze-thawing cycling compared with the static mechanical behavior.



**Figure 8.** Variation of dynamic strength with freezing temperature.

Corresponding to the impact pressure of 0.050, 0.055, and 0.060 MPa, the strain rates on specimens are approximately 38.97, 69.62, and 89.02  $s^{-1}$ . Figure 9 shows the effect of strain rate on dynamic strength of specimen experiencing 10-times freeze-thaw cycling treatments with a freezing temperature of  $-40$  °C. It is seen that a higher strain rate can induce a higher dynamic strength. Compared with the dynamic strength at the strain rate of 38.97  $s^{-1}$ , the dynamic strengths at the strain rates of 69.62 and 89.02  $s^{-1}$  increase by 23.4% and 42.1%, respectively.



**Figure 9.** Variation of dynamic strength with strain rate.

### 3.5. Effects of Freezing Temperature and Strain Rate on Dynamic Energy Absorption

The relationship between the dynamic energy absorption and freezing temperature during the freeze-thaw cycling process is shown in Figure 10. As the freezing temperature decreases, dynamic energy absorption decreases. Compared with the dynamic energy absorption of sandstone specimens at 20 °C, the dynamic energy absorption of sandstone specimens at the freezing temperature of  $-20$ ,  $-40$ ,  $-50$  °C, and  $-60$  °C decreases by 12.5%, 24.2%, 26.3%, and 30.7%, respectively. This phenomenon indicates that the energy consumed per unit volume of the sample decreases as the temperature decreases.

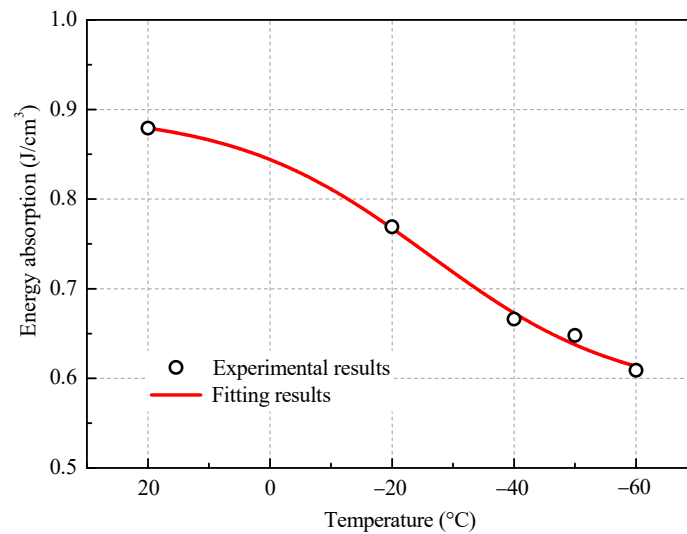


**Figure 10.** Variation of dynamic energy absorption with freezing temperature.

Figure 11 shows the effect of strain rate on dynamic energy absorption of specimens experiencing 10-times freeze-thaw cycling treatments with the freezing temperature of  $-40\text{ }^{\circ}\text{C}$ . It is seen from Figure 11 that as strain rate increases, dynamic energy absorption of sandstone specimens increases. Compared with the dynamic energy absorption at the strain rate of  $38.97\text{ s}^{-1}$ , the dynamic energy absorption of sandstone specimens at the strain rates of  $69.62$  and  $89.02\text{ s}^{-1}$  increases by  $76.3\%$  and  $126.3\%$ , respectively.

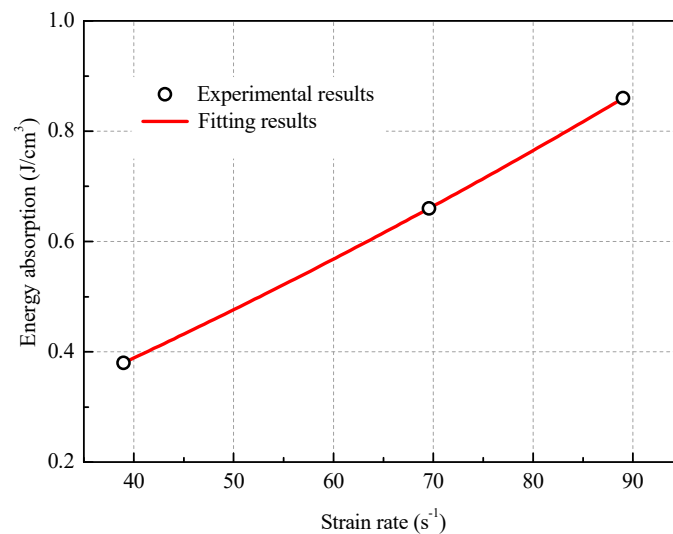


**Figure 11.** Variation of dynamic energy absorption with strain rate.

The decrease in the density, P-wave velocity, and mechanical strength of sandstone may be closely related to the generation and accumulation of micro-defects. Water weakening effects, inconsistent shrinkage and expansion between mineral grains and frost heave effects may induce the generation and accumulation of micro-defects. For the saturated specimens, the chemical and physical reactions between the water and clay minerals may occur, which may weaken the connection between mineral grains [17]. During freeze-thaw cycling, the decrease and increase in the temperature induce the shrinkage and expansion of mineral grains. The inconsistent shrinkage and expansion between mineral grains induce the generation of stress [48]. The repeated shrinkage and expansion of the mineral grains may induce the generation and accumulation of the micro-defects during freeze-thaw cycling [13]. During freezing, water in pores turns into ice, and the volume expansion due

to the water–ice phase transition may induce the generation of the frost heave force. When the frost heave force exceeds the strength of the material, cracking occurs [2].

The generation and accumulation of the micro-defects may induce the shedding of mineral grains due to a decrease in cohesion between the mineral grains, which further induces a decrease in the mass of the specimen [4]. Therefore, the density is calculated by the mass decreases.

When ultrasonic waves propagate in rock with micro-defects, the micro-defects can filter the harmonic components of waves with higher frequencies. The dominant frequency of the incident wave decreases, which further decreases the velocity [49–51]. The existence of the micro-defects decreases the mechanical strength of rock, increases the displacement deformation space during loading, and decreases the static elastic modulus [33,52]. In addition, the existence of the micro-defects decreases the energy required for fracturing a specimen. The micro-defects induced by the inconsistent deformation between mineral grains may increase as the freezing temperature during freeze-thaw cycling decreases. In addition, the damage induced by the frost heave effect increases as the freezing temperature decreases below a certain critical temperature [19]. Moreover, during thawing, water immersion may increase the deterioration. These factors may induce the decrease in the P-wave velocity, static uniaxial strength, static elastic modulus, dynamic strength, and dynamic energy absorption with the decrease in the freezing temperature.

The dynamic strength and dynamic energy absorption increase monotonically as the strain rate increases. During dynamic loading, the material may not have enough time to absorb energy because of the instantaneity of the impact, and the external energy can only be offset by increasing the stress. Therefore, the dynamic strength increases as the strain rate increases. The failure of the sandstone specimen is mainly caused by the initiation and propagation of cracks. As the strain rate increases, more cracks are generated, and the required energy correspondingly increases. Therefore, the dynamic energy absorption increases as the strain rate increases [53].

#### 4. Conclusions

In the present study, the degradation of mechanical behaviors of sandstone with freezing temperature under repeated freezing and thawing conditions was investigated. Under the same freeze-thaw cycling number (10 times), the effects of freezing temperature (−20, −40, −50, and −60 °C) on the density, P-wave velocity, static and dynamic uniaxial compressive strength, static elastic modulus, and dynamic energy absorption were discussed. The conclusions obtained are as follows.

- (1) The density of sandstone decreases as the freezing temperature decreases from 20 to −60 °C, and the decreasing extent of density approximately reaches 1.0% at −60 °C. The P-wave velocity first shows a slightly decreasing trend as the freezing temperature decreases, and then rapidly decreases after −20 °C.
- (2) Under the same freeze-thaw cycling number, the static uniaxial compressive strength, static elastic modulus, dynamic strength, and dynamic energy absorption of sandstone all decrease non-linearly as the freezing temperature decreases from 20 to −60 °C. However, the dynamic mechanical behavior is more sensitive to the freezing temperature during freeze-thawing cycling compared with the static mechanical behavior.
- (3) The strain rate significantly influences the dynamic mechanical responses of sandstone after low-temperature treatments. The dynamic strength and dynamic energy absorption increase monotonically as the strain rate increases.

The present study is mainly focused on the macroscopic mechanical behaviors of sandstone. Further research shall be conducted on the micro-scale to show its microscopic mechanisms.

**Author Contributions:** Conceptualization, J.G. and L.F.; Methodology, J.G. and C.X.; Data analysis, J.G. and C.X.; Writing-original draft preparation, J.G.; Writing-review and editing, L.F., J.G. and Y.X.; Funding acquisition, L.F. All authors have read and agreed to the published version of the manuscript.

**Funding:** The research is supported by the National Natural Science Foundation of China (NSFC) (No. 12172019 and 41831281) and Beijing Natural Science Foundation (JQ20039).

**Institutional Review Board Statement:** Not applicable.

**Informed Consent Statement:** Not applicable.

**Conflicts of Interest:** The authors declare no conflict of interest.

## References

- Wang, P.; Xu, J.Y.; Liu, S.; Wang, H.Y.; Liu, S.H. Static and dynamic mechanical properties of sedimentary rock after freeze-thaw or thermal shock weathering. *Eng. Geol.* **2016**, *210*, 148–157. [[CrossRef](#)]
- Deprez, M.; De Kock, T.; De Schutter, G.; Cnudde, V. A review on freeze-thaw action and weathering of rocks. *Earth-Sci. Rev.* **2020**, *203*, 103143. [[CrossRef](#)]
- Luo, Y.; Qu, D.X.; Wang, G.; Li, X.P.; Zhang, G. Degradation model of the dynamic mechanical properties and damage failure law of sandstone under freeze-thaw action. *Soil Dyn. Earthq. Eng.* **2020**, *132*, 106094. [[CrossRef](#)]
- Luo, X.D.; Jiang, N.; Zuo, C.Q.; Dai, Z.W.; Yan, S.T. Damage characteristics of altered and unaltered diabbases subjected to extremely cold freeze-thaw cycles. *Rock Mech. Rock Eng.* **2014**, *47*, 1997–2004. [[CrossRef](#)]
- Fang, X.Y.; Xu, J.Y.; Wang, P.X. Compressive failure characteristics of yellow sandstone subjected to the coupling effects of chemical corrosion and repeated freezing and thawing. *Eng. Geol.* **2018**, *233*, 160–171. [[CrossRef](#)]
- Inada, Y.; Yokota, K. Some studies of low temperature rock strength. *Int. J. Rock Mech. Min. Sci.* **1984**, *21*, 145–153. [[CrossRef](#)]
- Yamabe, T.; Neaupane, K.M. Determination of some thermo-mechanical properties of Sirahama sandstone under subzero temperature condition. *Int. J. Rock Mech. Min. Sci.* **2001**, *38*, 1029–1034. [[CrossRef](#)]
- Kodama, J.; Goto, T.; Fujii, Y.; Hagan, P. The effects of water content, temperature and loading rate on strength and failure process of frozen rocks. *Int. J. Rock Mech. Min. Sci.* **2013**, *62*, 1–13. [[CrossRef](#)]
- Bai, Y.; Shan, R.L.; Ju, Y.; Wu, Y.X.; Sun, P.F.; Wang, Z.E. Study on the mechanical properties and damage constitutive model of frozen weakly cemented red sandstone. *Cold Reg. Sci. Technol.* **2020**, *171*, 102980. [[CrossRef](#)]
- Dwivedi, R.D.; Soni, A.K.; Goel, R.K.; Dube, A.K. Fracture toughness of rocks under sub-zero temperature conditions. *Int. J. Rock Mech. Min. Sci.* **2000**, *37*, 1267–1275. [[CrossRef](#)]
- Yang, R.S.; Fang, S.Z.; Guo, D.M.; Li, W.Y.; Mi, Z.Z. Study on dynamic tensile strength of red sandstone under impact loading and negative temperature. *Geotech. Geol. Eng.* **2019**, *37*, 4527–4537. [[CrossRef](#)]
- Yang, R.S.; Fang, S.Z.; Li, W.Y.; Yang, Y.; Yue, Z.W. Experimental study on the dynamic properties of three types of rock at negative temperature. *Geotech. Geol. Eng.* **2019**, *37*, 455–464. [[CrossRef](#)]
- Weng, L.; Wu, Z.J.; Liu, Q.S. Dynamic mechanical properties of dry and water-saturated siltstones under sub-zero temperatures. *Rock Mech. Rock Eng.* **2020**, *53*, 4381–4401. [[CrossRef](#)]
- Mardoukhi, A.; Mardoukhi, Y.; Hokka, M.; Kuokkala, V.T. Effects of test temperature and low temperature thermal cycling on the dynamic tensile strength of granitic rocks. *Rock Mech. Rock Eng.* **2021**, *54*, 443–454. [[CrossRef](#)]
- Kurilko, A.S.; Novopashin, M.D. Features of low temperature effect upon strength of enclosing rock and kimberlite in the “Udachnaya” pipe. *J. Min. Sci.* **2005**, *41*, 119–122. [[CrossRef](#)]
- Zakharov, E.V.; Kurilko, A.S. Effects of low temperatures on strength and power input into rock failure. *Sci. Cold Arid. Reg.* **2014**, *6*, 455–460. [[CrossRef](#)]
- Vasarhelyi, B. Statistical analysis of the influence of water content on the strength of the miocene limestone. *Rock Mech. Rock Eng.* **2005**, *38*, 69–76. [[CrossRef](#)]
- Weng, L.; Wu, Z.J.; Liu, Q.S.; Wang, Z.Y. Energy dissipation and dynamic fragmentation of dry and water-saturated siltstones under sub-zero temperatures. *Eng. Fract. Mech.* **2019**, *220*, 106659. [[CrossRef](#)]
- Jia, H.L.; Zi, F.; Yang, G.S.; Li, G.Y.; Shen, Y.J.; Sun, Q.; Yang, P.Y. Influence of pore water (ice) content on the strength and deformability of frozen argillaceous siltstone. *Rock Mech. Rock Eng.* **2020**, *53*, 967–974. [[CrossRef](#)]
- Tan, X.J.; Chen, W.Z.; Yang, J.P.; Cao, J.J. Laboratory investigations on the mechanical properties degradation of granite under freeze-thaw cycles. *Cold Reg. Sci. Technol.* **2011**, *68*, 130–138. [[CrossRef](#)]
- Mu, J.Q.; Pei, X.J.; Huang, R.Q.; Rengers, N.; Zou, X.Q. Degradation characteristics of shear strength of joints in three rock types due to cyclic freezing and thawing. *Cold Reg. Sci. Technol.* **2017**, *138*, 91–97. [[CrossRef](#)]
- Celik, M.Y. Water absorption and P-wave velocity changes during freeze-thaw weathering process of crosscut travertine rocks. *Environ. Earth Sci.* **2017**, *76*, 409. [[CrossRef](#)]

23. Liu, C.J.; Deng, H.W.; Zhao, H.T.; Zhang, J. Effects of freeze-thaw treatment on the dynamic tensile strength of granite using the Brazilian test. *Cold Reg. Sci. Technol.* **2018**, *155*, 327–332. [[CrossRef](#)]
24. Zhang, J.; Deng, H.W.; Taheri, A.; Ke, B.; Liu, C.J.; Yang, X.R. Degradation of physical and mechanical properties of sandstone subjected to freeze-thaw cycles and chemical erosion. *Cold Reg. Sci. Technol.* **2018**, *155*, 37–46. [[CrossRef](#)]
25. Weng, L.; Wu, Z.J.; Taheri, A.; Liu, Q.S.; Lu, H. Deterioration of dynamic mechanical properties of granite due to freeze-thaw weathering: Considering the effects of moisture conditions. *Cold Reg. Sci. Technol.* **2020**, *176*, 103092. [[CrossRef](#)]
26. Ma, Q.Y.; Ma, D.D.; Yao, Z.M. Influence of freeze-thaw cycles on dynamic compressive strength and energy distribution of soft rock specimen. *Cold Reg. Sci. Technol.* **2018**, *153*, 10–17. [[CrossRef](#)]
27. Fan, L.F.; Xu, C.; Wu, Z.J. Effects of cyclic freezing and thawing on the mechanical behavior of dried and saturated sandstone. *Bull. Eng. Geol. Environ.* **2020**, *79*, 755–765. [[CrossRef](#)]
28. Park, J.; Hyun, C.U.; Park, H.D. Changes in microstructure and physical properties of rocks caused by artificial freeze-thaw action. *Bull. Eng. Geol. Environ.* **2015**, *74*, 555–565. [[CrossRef](#)]
29. Liu, B.; Ma, Y.J.; Liu, N.; Han, Y.H.; Li, D.Y.; Deng, H.L. Investigation of pore structure changes in Mesozoic water-rich sandstone induced by freeze-thaw process under different confining pressures using digital rock technology. *Cold Reg. Sci. Technol.* **2019**, *161*, 137–149. [[CrossRef](#)]
30. Zhang, J.; Deng, H.W.; Deng, J.R.; Guo, H.Q. Influence of freeze-thaw cycles on the degradation of sandstone after loading and unloading. *Bull. Eng. Geol. Environ.* **2020**, *79*, 1967–1977. [[CrossRef](#)]
31. Hall, K. The role of thermal stress fatigue in the breakdown of rock in cold regions. *Geomorphology* **1999**, *31*, 47–63. [[CrossRef](#)]
32. Ishikawa, M.; Kurashige, Y.; Hirakawa, K. Analysis of crack movements observed in an alpine bedrock cliff. *Earth Surf. Proc. Land.* **2004**, *29*, 883–891. [[CrossRef](#)]
33. Liu, C.J.; Deng, J.R.; Yu, S.T.; Li, P.; Lin, Y. Effect of freezing and thawing on microstructure damage and dynamic flexural tension of granite. *Rock Mech. Rock Eng.* **2020**, *53*, 3853–3858. [[CrossRef](#)]
34. Liu, Y.Z.; Cai, Y.T.; Huang, S.B.; Guo, Y.L.; Liu, G.F. Effect of water saturation on uniaxial compressive strength and damage degree of clay-bearing sandstone under freeze-thaw. *Bull. Eng. Geol. Environ.* **2020**, *79*, 2021–2036. [[CrossRef](#)]
35. Luo, X.D.; Zhou, S.T.; Huang, B.; Jiang, N.; Xiong, M.X. Effect of freeze-thaw temperature and number of cycles on the physical and mechanical properties of marble. *Geotech. Geol. Eng.* **2020**, *39*, 567–582. [[CrossRef](#)]
36. Abdolghanizadeh, K.; Hosseini, M.; Saghafiyaadi, M. Effect of freezing temperature and number of freeze-thaw cycles on mode I and mode II fracture toughness of sandstone. *Theor. Appl. Fract. Mech.* **2020**, *105*, 102428. [[CrossRef](#)]
37. Fan, L.F.; Wang, M.; Wu, Z.J. Effect of nonlinear deformational macrojoint on stress wave propagation through a double-scale discontinuous rock mass. *Rock Mech. Rock Eng.* **2021**, *54*, 1077–1090. [[CrossRef](#)]
38. Fan, L.F.; Yang, K.C.; Wang, M.; Wang, L.J.; Wu, Z.J. Experimental study on wave propagation through granite after high-temperature treatment. *Int. J. Rock Mech. Min. Sci.* **2021**, *148*, 104946. [[CrossRef](#)]
39. Bieniawski, Z.T.; Bernede, M.J. Suggested methods for determining the uniaxial compressive strength and deformability of rock materials. 1. Suggested method for determination of the uniaxial compressive strength of rock materials. *Int. J. Rock Mech. Min. Sci.* **1979**, *16*, 137–138. [[CrossRef](#)]
40. Zhou, Y.X.; Xia, K.; Li, X.B.; Li, H.B.; Ma, G.W.; Zhao, J.; Zhou, Z.L.; Dai, F. Suggested methods for determining the dynamic strength parameters and mode-I fracture toughness of rock materials. *Int. J. Rock Mech. Min. Sci.* **2012**, *49*, 105–112. [[CrossRef](#)]
41. Yang, S.Q.; Huang, Y.H.; Tian, W.L.; Ying, P.F.; Jing, H.W. Effect of high temperature on deformation failure behavior of granite specimen containing a single fissure under uniaxial compression. *Rock Mech. Rock Eng.* **2019**, *52*, 2087–2107. [[CrossRef](#)]
42. Fan, L.F.; Gao, J.W.; Wu, Z.J.; Yang, S.Q.; Ma, G.W. An investigation of thermal effects on micro-properties of granite by X-ray CT technique. *Appl. Therm. Eng.* **2018**, *140*, 505–519. [[CrossRef](#)]
43. Sun, H.; Sun, Q.; Deng, W.N.; Zhang, W.Q.; Lv, C. Temperature effect on microstructure and P-wave propagation in Linyi sandstone. *Appl. Therm. Eng.* **2017**, *115*, 913–922. [[CrossRef](#)]
44. Zhou, Z.L.; Li, X.B.; Ye, Z.Y.; Liu, K.W. Obtaining constitutive relationship for rate-dependent rock in SHPB tests. *Rock Mech. Rock Eng.* **2010**, *43*, 697–706. [[CrossRef](#)]
45. Li, Y.B.; Zhai, Y.; Wang, C.S.; Meng, F.D.; Lu, M. Mechanical properties of Beishan granite under complex dynamic loads after thermal treatment. *Eng. Geol.* **2020**, *267*, 105481. [[CrossRef](#)]
46. Gao, J.W.; Xi, Y.; Fan, L.F.; Du, X.L. Real-time visual analysis of the microcracking behavior of thermally damaged granite under uniaxial loading. *Rock Mech. Rock Eng.* **2021**, 1–16. [[CrossRef](#)]
47. Li, J.L.; Kaunda, R.B.; Zhou, K.P. Experimental investigations on the effects of ambient freeze-thaw cycling on dynamic properties and rock pore structure deterioration of sandstone. *Cold Reg. Sci. Technol.* **2018**, *154*, 133–141. [[CrossRef](#)]
48. Fan, L.F.; Gao, J.W.; Du, X.L.; Wu, Z.J. Spatial gradient distributions of thermal shock-induced damage to granite. *J. Rock Mech. Geotech.* **2020**, *12*, 917–926. [[CrossRef](#)]
49. Ma, G.W.; Fan, L.F.; Li, J.C. Evaluation of equivalent medium methods for stress wave propagation in jointed rock mass. *Int. J. Numer. Anal. Methods Geomech.* **2013**, *37*, 701–715. [[CrossRef](#)]
50. Fan, L.F.; Wu, Z.J.; Wan, Z.; Gao, J.W. Experimental investigation of thermal effects on dynamic behavior of granite. *Appl. Therm. Eng.* **2017**, *125*, 94–103. [[CrossRef](#)]

51. Qin, Y.; Tian, H.; Xu, N.X.; Chen, Y. Physical and mechanical properties of granite after high-temperature treatment. *Rock Mech. Rock Eng.* **2020**, *53*, 305–322. [[CrossRef](#)]
52. Xu, J.C.; Pu, H.; Sha, Z.H. Mechanical behavior and decay model of the sandstone in Urumqi under coupling of freeze-thaw and dynamic loading. *Bull. Eng. Geol. Environ.* **2021**, *80*, 2963–2978. [[CrossRef](#)]
53. Feng, S.W.; Zhou, Y.; Wang, Y.; Lei, M.D. Experimental research on the dynamic mechanical properties and damage characteristics of lightweight foamed concrete under impact loading. *Int. J. Impact Eng.* **2020**, *140*, 103558. [[CrossRef](#)]